


Article

# Fatigue Analysis of Inter-Array Power Cables between Two Floating Offshore Wind Turbines Including a Simplified Method to Estimate Stress Factors

Dennis Beier <sup>1</sup>, Anja Schnepf <sup>1,2</sup>, Sean Van Steel <sup>3</sup>, Naiquan Ye <sup>4</sup> and Muk Chen Ong <sup>1,\*</sup> 

<sup>1</sup> Department of Mechanical and Structural Engineering and Materials Science, University of Stavanger, 4036 Stavanger, Norway; dennis.beier@gmx.net (D.B.); anja.schnepf@uis.no (A.S.)

<sup>2</sup> CoreMarine, 4014 Stavanger, Norway

<sup>3</sup> CoreMarine, Hobart, TAS 7000, Australia; sv@s-core-marine.com

<sup>4</sup> SINTEF Ocean, 7052 Trondheim, Norway; naiquan.ye@sintef.no

\* Correspondence: muk.c.ong@uis.no

**Abstract:** The use of floating offshore wind farms for electrical energy supply is expected to rise significantly over the coming years. Suspended inter-array power cables are a new design to connect floating offshore wind turbines (FOWTs) with shorter cable lengths than conventional setups. The present study investigates the fatigue life of a suspended power cable with attached buoys connecting two spar-type FOWTs. Typical environmental conditions for the North Sea are applied. The nonlinear bending behavior of the power cable is considered in the analysis. Fatigue assessment is performed using the numerical software OrcaFlex based on stress factors obtained from cross-section analysis. An effective method for obtaining the stress factors is proposed for early engineering design stages and compared with the finite element software UFLEX simulation results. The simplified method delivers similar results for axial tension loads and conservative results for bending loads compared with results obtained from the finite element software. Stress components resulting from curvature variation are identified as the main contributors to fatigue damage. The most critical locations along the power cable for fatigue life are close to the hang-off points.

**Keywords:** inter-array power cable; power umbilical; fatigue; floating offshore wind turbine; stress factors



**Citation:** Beier, D.; Schnepf, A.; Van Steel, S.; Ye, N.; Ong, M.C. Fatigue Analysis of Inter-Array Power Cables between Two Floating Offshore Wind Turbines Including a Simplified Method to Estimate Stress Factors. *J. Mar. Sci. Eng.* **2023**, *11*, 1254. <https://doi.org/10.3390/jmse11061254>

Academic Editor: José António Correia

Received: 5 May 2023

Revised: 5 June 2023

Accepted: 9 June 2023

Published: 20 June 2023



**Copyright:** © 2023 by the authors. Licensee MDPI, Basel, Switzerland. This article is an open access article distributed under the terms and conditions of the Creative Commons Attribution (CC BY) license (<https://creativecommons.org/licenses/by/4.0/>).

## 1. Introduction

To achieve the goal of limiting global warming to 1.5 °C set by the United Nations in the Paris Climate Agreement, renewable energy sources, including wind energy, must be extended in the future [1]. Since offshore locations have vast wind potential and are not as constrained by populated or protected areas as onshore locations, particularly offshore wind farms, they are expected to grow substantially [2]. While most offshore wind farms are bottom-fixed platforms installed in shallow waters, a few projects are already implemented in deeper waters, such as the floating wind farms Hywind Scotland, WindFloat Atlantic, and Hywind Tampen [3–5]. In all implemented projects, the power cables connecting the FOWTs are laid on the seabed [3–5]. However, the power cables can also be suspended, which means they are submerged but do not touch the seabed. These suspended configurations can reduce the length compared to cables laying on the seabed. This length reduction has the advantages of reduced inter-array energy loss and lower investment costs for the power cables [6]. This work analyzes the fatigue damage of suspended inter-array power cables between two floating offshore wind turbines using a stress factor-based fatigue analysis approach.

Ikhennicheu et al. [7] published various offshore dynamic power cable configurations connecting a floating platform and the seabed. The most common dynamic cable configurations described in the literature are the catenary and lazy-wave shapes. The lazy-wave

shape distinguishes itself from the catenary shape through buoyancy modules attached to the hanging power cable. Thies et al. [8] analyzed a dynamic umbilical's tension and fatigue life in lazy-wave and catenary configurations connecting a wave energy converter with a static power cable at the seabed. They showed that the lazy-wave configuration reduces the maximum tension and the number of fatigue cycles in the dynamic umbilical compared with the catenary configuration. A reduction in the maximum tension resulted in a significant extension of the fatigue life of the dynamic umbilical. Thies et al. [9] obtained the tensions and fatigue of a 66 kV cable connecting a FOWT to the seabed in a lazy-wave shape. The platform's motion was the main contributor to the loads on the umbilical. Rentschler et al. [6] presented a design optimization method for inter-array cable configurations for FOWTs. Their study included an estimation of the fatigue life, the performance in extreme weather conditions, and selected economic parameters for lazy-wave power umbilical configurations. They applied the method to dynamic umbilical configurations at different water depths, resulting in reduced buoyancy sections and a lower position of the wave shape than in the original design. Bakken [10] calculated the fatigue life of a dynamic power cable connecting a FOWT to the seabed using the numerical programs SIMA and Bflex. The lowest fatigue life occurred at the locations with the maximum tension range, and the main contributors to the fatigue of the copper conductor were local friction effects. Hu et al. [11] investigated the bending behavior of a copper conductor inside a dynamic power cable experimentally and numerically. They stated that the nonlinear bending of the power cable is the main factor leading to fatigue failures. Prediction models for the fatigue of dynamic power cables were developed by Svensson [12] using experiments and finite element simulations. Interlayer friction forces were an important factor in the calculation of the fatigue life of the power cable. Zhao et al. [13] studied the behavior and fatigue of power cables in lazy-wave and double-wave configurations connected to a FOWT in shallow water. They detected the hang-off point as the most critical point regarding the tension and fatigue of the power cable for both shapes. The second buoyancy section of the double wave configuration was critical for fatigue life. Ballard et al. [14] estimated the fatigue life of a lazy-wave-shaped umbilical attached to a wave energy converter. Curvature-induced fatigue was identified as the critical parameter in their setup, causing fatigue damage.

The general fatigue properties of a copper conductor inside a dynamic subsea power cable were determined by Karlsen et al. [15]. They suggested using strain-cycle curves for copper conductors due to the limited applicability of traditional S-N curves for this material. Marta et al. [16] assessed a dynamic power cable's stresses and fatigue life at floating offshore renewable energy installations. Fretting was identified as a major crack initiation mechanism in copper conductors, causing fatigue failure. The governing failure mode in all their cases was fatigue. Nasution et al. [17] established the S-N curve of a copper conductor of power cables used in offshore wind farms through experimental data and finite element simulations. Nasution et al. [18] assessed the effects of tension and bending loads on copper power conductors. They identified inter-layer friction caused by curvature as the main reason for fatigue failures.

Yang et al. [19] presented the dynamic motions and fatigue damage of a power cable connecting a wave energy converter to a static hub in a freely hanging catenary configuration. They calculated a long fatigue life for a simplified cable, disregarding internal effects such as wear or fretting. Suspended power cables between FOWTs were described by Rapha and Domínguez [20]. Schnepf et al. [21] performed feasibility studies for different suspended power cable configurations. They identified configurations with buoys as more suitable than configurations with buoyancy modules. The behavior of a suspended power cable connecting a FOWT with a floating production storage and offloading unit (FPSO) was analyzed by Schnepf et al. [22]. The results showed that suspended configurations with buoys attached evenly over the power cable length could reduce its tension compared to a freely hanging configuration and a configuration with buoys attached to its middle section. Ahmad et al. [23] proposed a design method for suspended inter-array power cable configurations between two FOWTs. They concluded that attaching several buoys

leads to lower maximum tensions in the power cable and that copper conductors might be more suitable for suspended power cables than aluminum conductors. To the authors' knowledge, no work has yet been performed assessing the fatigue of a suspended power cable. Analyzing the fatigue life of a suspended power cable due to dynamic loading is important for identifying possible design optimizations and ensuring the reliability and cost-effectiveness of the proposed setup. Additionally, no study has yet been published on a simplified method to obtain stress factors for calculating the fatigue of power cables.

This work is organized as follows: Section 2 describes the software used, the setup of the FOWTs and the connecting suspended power cable in deep water, the environmental conditions applied, and the fatigue assessment. Section 3 presents and discusses the results of the stress factor calculations and the fatigue analyses of the case study. Conclusions are drawn in Section 4.

## 2. Methodology and Numerical Setup

This section describes the applied software for the present study, the numerical setup of the suspended power cable configuration between two FOWTs, the environmental conditions, and the applied fatigue calculation method.

### 2.1. Numerical Tools

The present study uses the numerical software OrcaFlex version 11.2d [24] in combination with Python v3.10 [25]. This software can perform global static and dynamic analyses of marine systems, including analyses of the behavior of wind turbines. A time-domain solution procedure determines the interactions between floating structures and the environmental loads (including wave, wind, and current loads). Moreover, fatigue calculations can be carried out based on the results of dynamic simulations. Line structures such as power cables can be modeled with finite elements.

The finite element software UFLEX version 2.8 [26] is used to determine cable properties. The software assumes that the problem is two-dimensional with respect to tension and torsion, while bending loads, including their three-dimensional extent, are considered. Filled bodies can be modeled as beam elements and tubular bodies as shell elements. UFLEX provides modeling capabilities for complex cross-section geometries, contact and friction stresses, nonlinear relationships between curvature and bending moment, cross-section geometry ovalization, and nonlinear material models. This software has been validated by other finite element software as well as experiments described by Sævik and Bruaseth [27], Dai [28], Sævik and Gjøsteen [29], and SINTEF [30].

### 2.2. Numerical Models

This section describes the FOWT system, the properties of the dynamic power cable, and the setup of the suspended power cable configuration.

#### 2.2.1. Floating Offshore Wind Turbine System

The reference wind turbine in the present study is the 5MW OC3-Hywind FOWT based on Jonkman et al. [31] and Jonkman [32]. This FOWT uses a spar concept, and the stability of the platform is achieved through the large draft of the cylindrical buoy. Figure 1 shows the geometry of the FOWT, and Table 1 lists its general parameters. The setup of the FOWT in the dynamic analysis software is based on Schnepf et al. [21].

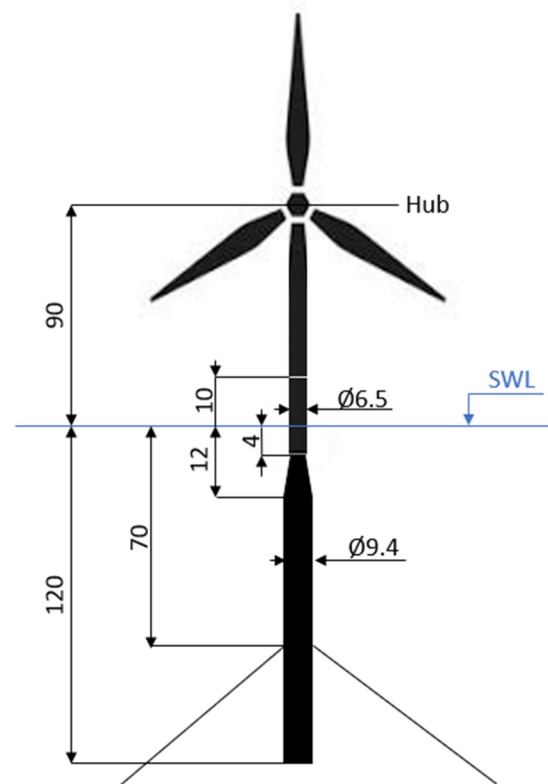


Figure 1. OC3-Hywind FOWT geometry. Dimensions in m.

Table 1. OC3-Hywind FOWT specifications (based on Jonkman [31,32]).

Rotor orientation, configuration	-	Upwind, 3 blades
Diameter rotor, hub	m	126, 3
Hub height	m	90
Platform total draft	m	120
Number of mooring lines	-	3
Angle between mooring lines	°	120
Water depth	m	320
Cut-in, rated, cut-out wind speed	m/s	3, 11.4, 25

### 2.2.2. Power Cable Properties

This study uses a 66 kV dynamic power cable designed by Nexans [33]. Table 2 describes the general properties of the power cable, and Figure 2 shows its cross-section. The cable contains three copper conductors consisting of 19 copper wires, accumulating to a total copper cross-sectional area of 285 mm<sup>2</sup>. Two layers of armored steel wires with a diameter of 4.2 mm are used to protect and stabilize the cable. The helically laid armor wires have a lay angle of 10° and −10°, respectively. A lay angle of 10° is used for the entire copper conductor, while the second and third copper wire layers have lay angles of 2° and 4°, respectively. The remaining insulation and binding components are made of polymer materials, such as cross-linked polyethylene (XLPE). Table 3 describes the material properties of the different cable components. The fiber-optic wire shown in the cable cross-section is neglected in the present study based on the procedures of previous works such as Thies et al. [8], Rentschler et al. [6], and Svensson [12]. Figure 3 shows the copper wires' stress–cycle curve (S–N curve) in the dynamic umbilical. The curve is similar to the one obtained by Nasution et al. [17]. The S–N curve for the armor steel wires is shown in Figure 3. It is similar to the S–N curves for steel with cathodic protection provided by DNV [34]. This study uses S–N curves and not strain-cycle curves as proposed by Karlsen et al. [15], based on the procedures of the majority of similar studies, such as

Marta et al. [16], Ballard et al. [14], and Nasution et al. [18]. Power cable manufacturers, such as Nexans, usually only provide S–N curves for their products under the current standard engineering approach [33].

**Table 2.** Power cable properties (Nexans [33] and DNV [34]).

Core main material	–	Copper
Voltage rating	kV	66
Outer diameter	m	0.116
Mass per unit length	kg/m	25.0
Length	m	1260
Torsional stiffness	kNm <sup>2</sup>	38.0
Axial stiffness	MN	362
Tension at conductor yield	kN	885
Minimum bending radius	m	1.8
Drag coefficient	–	1.2
Added mass coefficient	–	1.0

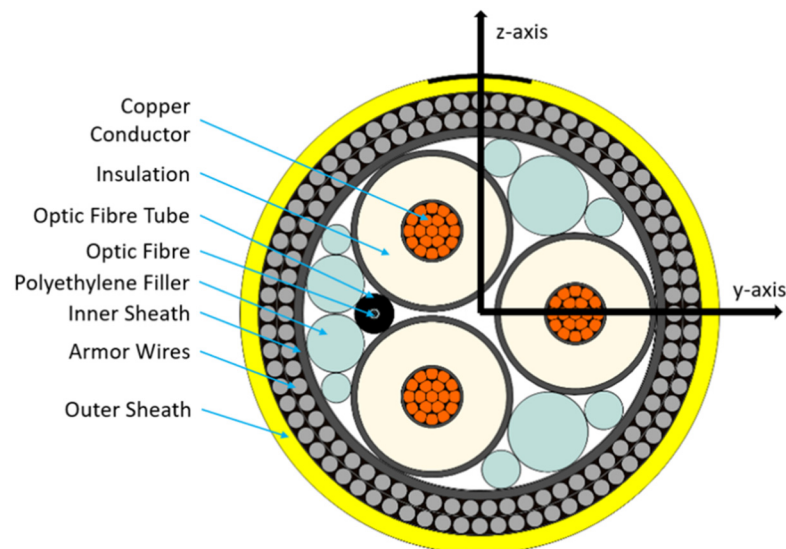


**Figure 2.** Power cable cross-section (reproduced from Nexans [33]).

**Table 3.** Material properties of the power cable components.

Material	Density (kg/m <sup>3</sup> )	Young’s Modulus (MPa)	Poisson’s Ratio (–)
Copper	8900	95,000	0.30
Steel	7800	200,000	0.30
XLPE	950	800	0.45

The power cable’s diameter and weight increase during its lifetime because marine growth is dependent on the water depth. The calculation of the marine growth effects in this study is based on the information given by NORSOK [35] and DNV [36]. The start-of-life (SOL) state and the end-of-life (EOL) state power cable properties are specified in Table 4.

**Table 4.** Power cable properties with marine growth.

Marine Growth State	Water Depth (m)	Outer Diameter (m)	Mass per Unit Length (kg/m)
SOL	Below −100	0.116	25.0
EOL1	−100 to −60	0.156	34.4
EOL2	−60 to −50	0.176	40.1

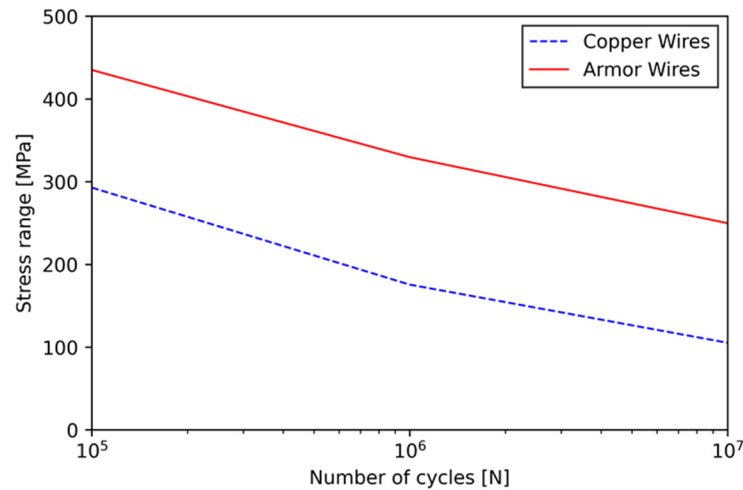


**Figure 3.** S–N curve for the power cable components (Nexans [33]).

### 2.2.3. Suspended Power Cable Setup

The inter-array power cable is suspended between the two FOWTs without touching the seabed or sea surface. Figure 4 shows an example of a suspended power cable setup. The distance between the wind turbines is 1134 m, equivalent to 9 times the rotor diameter of the FOWTs. The power cable is 1260 m long and divided into sections of different discretization sizes. A section of 10 m from the hang-off location has a segment length of 0.1 m, and the free-hanging cable sections have a segment length of 1.0 m. Attached to the power cable are three buoys with a distance of 300 m between them. The properties of the buoys are described in Table 5. The buoys have an anti-marine growth coating. Bend stiffeners to prevent excessive cable bending are attached to both ends of each buoy. The cable is discretized with a segment length of 0.31 m at the subsea buoys and 0.12 m at the bend stiffeners. The power cable hang-off consists of an I-tube, as shown in Figure 5. The center of its bell mouth is 70 m below the still-sea water level (SWL) at an 8 m radius from the spar center axis. It has a length of 7 m and is placed at an angle of 25° from the spar. The bell mouth opening has a diameter of 2.3 m and a minimum radius of 1.9 m. The mooring systems of the two FOWTs are mirrored, as shown in Figure 6. The nacelles of the wind turbines are always rotated towards the incoming wind direction.

**Table 5.** Properties of the buoys (Ahmad et al. [23]).

Length	m	2.170
Volume	m <sup>3</sup>	8.615
Mass	kg	2700
Equivalent buoy outer diameter (cylinder shape)	m	2.248
Drag coefficient (normal)	–	0.209
Drag coefficient (axial)	–	1.000
Added mass coefficient (normal)	–	0.459
Added mass coefficient (axial)	–	0.600



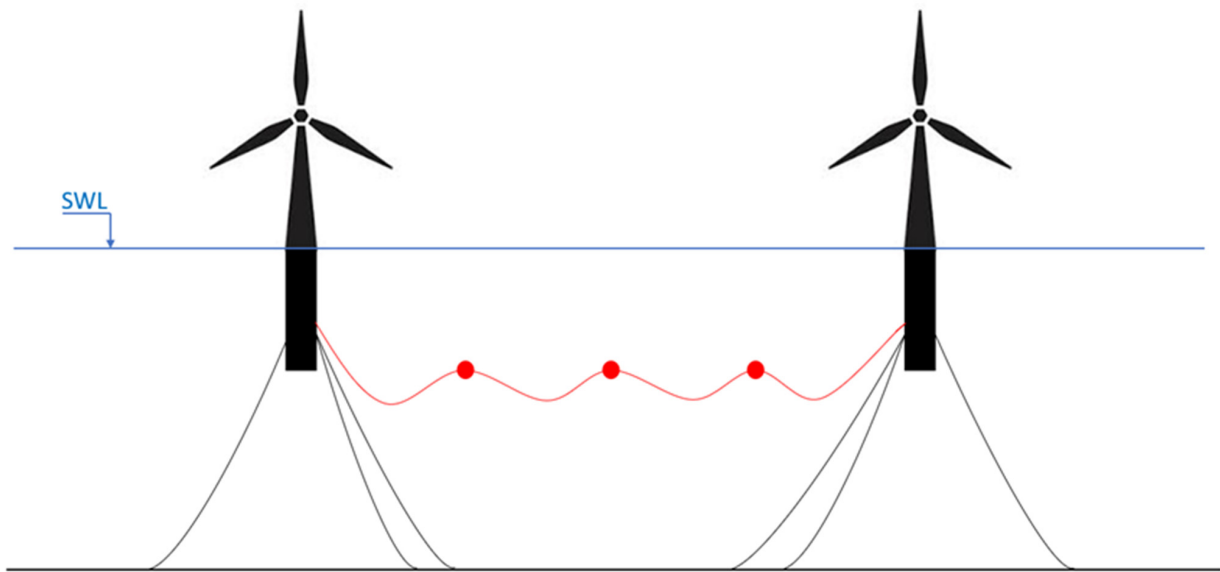


Figure 4. Concept of two FOWTs with a suspended power cable.

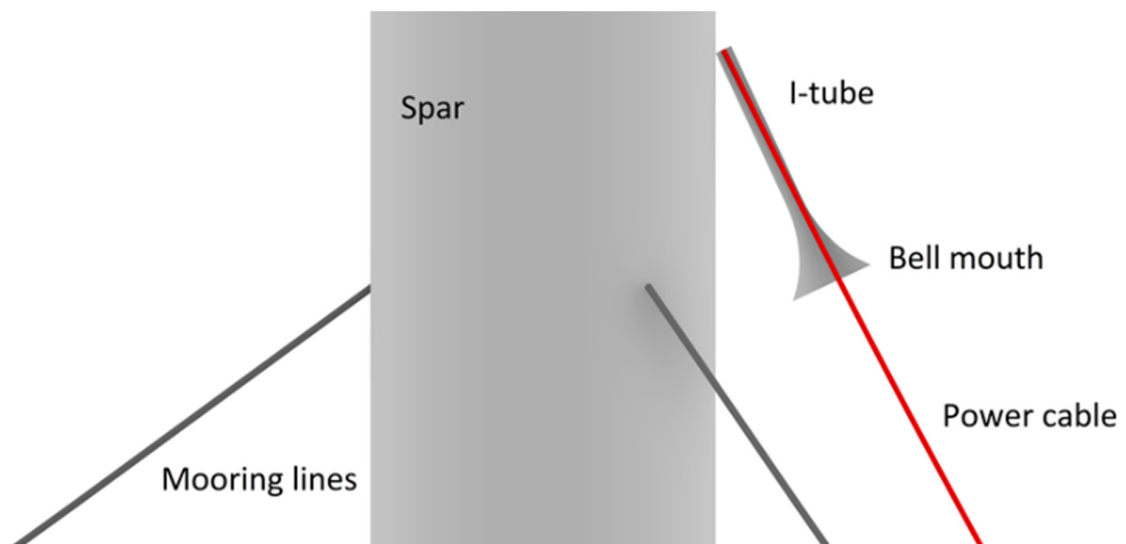


Figure 5. Power cable hang-off detail.

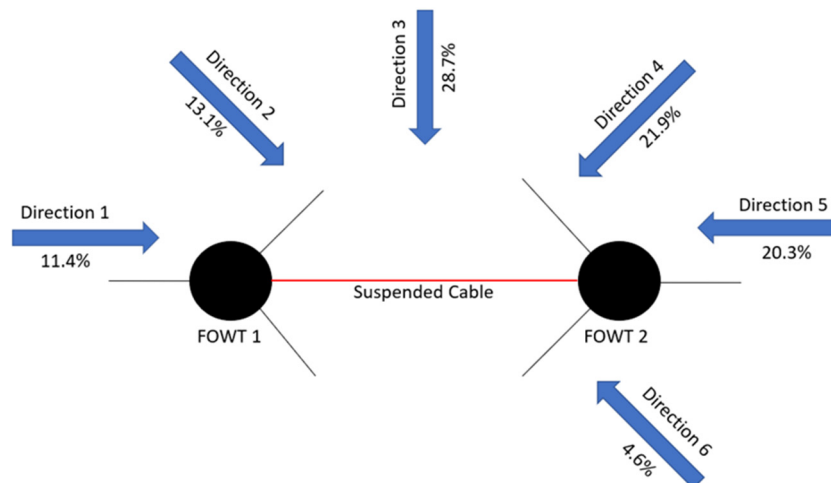


Figure 6. Loading directions on the suspended power cable system.

### 2.3. Environmental Conditions

The wave, wind, and current conditions are based on a location in the North Sea on a latitude of 61° N with a water depth of 320 m from Spyrou et al. [37], Komen et al. [38], WAMDI [39], Papadopoulos et al. [40], and Asplin et al. [41]. Table 6 presents all environmental parameters for the 30 load cases used in the present study, along with their occurrence probabilities. Load case 30 represents extreme weather when the wind turbine is idling. The FOWT is in operation in all other load cases. The Torsethaugen spectrum is applied to model irregular waves, and the NPD spectrum is used to simulate the wind [24]. The current velocity at a specific height  $z$  is estimated through the following formula given by DNV [36]:

$$v_c(z) = v_{c,SWL}(0) \left( \frac{d+z}{d} \right)^{\frac{1}{7}} \tag{1}$$

where  $v_{c,SWL}$  is the current velocity at the still water level, and  $d$  is the water depth. The six directions of the environmental loads toward the power cable and their appearance probabilities are shown in Figure 7. Wind and waves are aligned in all load cases to obtain conservative results.

**Table 6.** Environmental data.

Load	Wave Hs	Wave Tp	Current at SWL	Windspeed at Hub Height	Probabilities
case	(m)	(s)	(m/s)	(m/s)	
1	1.2	8.3	0.06	3.7	21.0%
2	0.9	9.9	0.12	7.5	5.09%
3	0.9	4.0	0.12	7.5	3.33%
4	1.9	13.5	0.12	7.5	7.56%
5	1.9	11.7	0.12	7.5	10.56%
6	3.0	11.8	0.15	9.4	5.80%
7	3.0	13.6	0.15	9.4	7.08%
8	1.0	15.0	0.15	10.4	2.39%
9	3.8	8.0	0.17	10.4	2.50%
10	4.5	13.4	0.18	11.4	3.84%
11	1.9	6.4	0.18	11.4	4.12%
12	3.7	10.0	0.18	11.4	4.10%
13	4.0	6.3	0.2	12.9	0.90%
14	1.8	8.2	0.2	12.9	1.60%
15	4.0	10.1	0.2	12.9	4.09%
16	4.0	11.6	0.2	12.9	1.66%
17	4.0	13.2	0.2	12.9	1.07%
18	1.3	17.1	0.2	12.9	0.43%
19	3.3	8.1	0.24	14.9	1.97%
20	3.9	15.3	0.24	14.9	2.99%
21	3.9	17.0	0.24	14.9	0.16%
22	5.9	9.1	0.28	17.7	0.84%
23	5.9	11.4	0.28	17.7	1.43%
24	5.9	12.0	0.28	17.7	1.37%
25	5.9	14.9	0.28	17.7	1.33%
26	7.4	9.8	0.35	21.5	0.22%
27	8.5	11.5	0.35	21.5	0.81%
28	9.0	13.7	0.35	21.5	1.53%
29	9.0	16.0	0.35	21.5	0.10%
30	11.9	13.8	0.47	30	0.13%



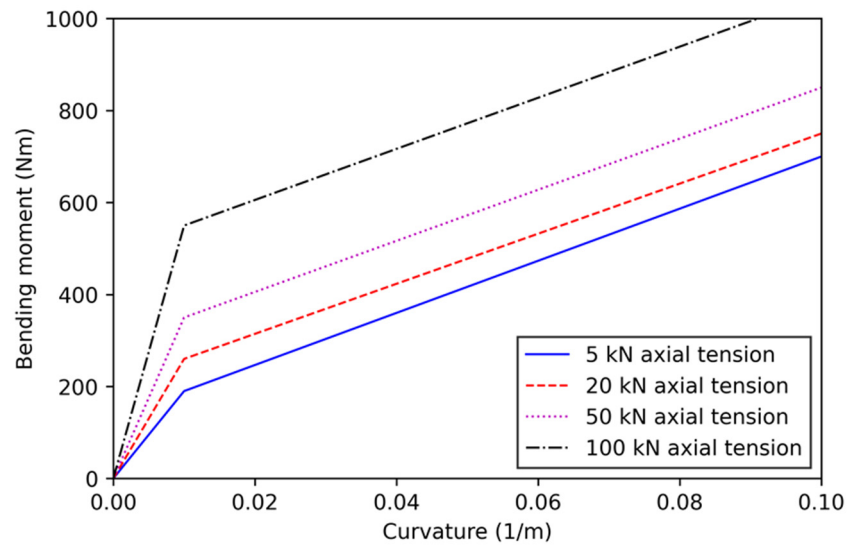


Figure 7. Nonlinear bending behavior of the power cable for different axial tension levels.

#### 2.4. Fatigue Assessment

The fatigue assessment in this study is carried out in four steps. First, the nonlinear bending behavior of the power cable is determined. Second, dynamic analyses of the entire setup are performed to obtain the axial tension and the bending curvatures of the power cable. Third, the stresses of the cable components are calculated through stress factors. This work proposes a simplified and effective method to estimate these stress factors for dynamic power cables. Fourth, fatigue damage is determined by applying the rainflow counting method and the Miner–Palmgren rule.

##### 2.4.1. Nonlinear Bending Behavior Estimation

Dynamic power cables show nonlinear bending behavior due to friction, contact, and slip effects between the wires in the same layer and between wires of different layers [11]. The nonlinear bending behavior of the power cable is determined through finite-element analysis in UFLEX. A stepwise curvature is applied to the cable, and each step’s corresponding bending moment is calculated. The obtained relationship between the bending curvature and the bending moment is applied to the power cable in the dynamic analyses.

##### 2.4.2. Calculation of Stresses Using Stress Factors

The stresses to determine damage are obtained by the following formula [24]:

$$S = K_t T + K_c (C_x \sin\theta - C_y \cos\theta) \tag{2}$$

where  $S$  is the stress and  $K_t$  and  $K_c$  are the tension and curvature stress factors.  $T$  is the effective tension,  $C_x$  and  $C_y$  are the curvature components, and  $\theta$  is the circumferential location of the fatigue point.

In the following part, this study proposes a simplified method for estimating the stress factors in a dynamic power cable in the early design stages when results from validated software or experiments are unavailable. If the power cable has a relatively low axial tension but a high bending utilization during its operation, the tension stress factors can be derived using the equations for the simple area stress of composite beams. When axially loaded, the strain is continuous across the cross-section of a composite beam, but the stress is discontinuous [42]. From Hook’s law, the following can be deduced for a beam with two components when an axial load is applied:

$$\varepsilon = \sigma_1 / E_1 = \sigma_2 / E_2 \tag{3}$$

where  $\varepsilon$  is the strain and  $\sigma_1$  and  $\sigma_2$  are the axial stresses of cable components 1 and 2.  $E_1$  and  $E_2$  are Young's moduli of the respective cable components. The tension must equal the stresses times their respective areas in the longitudinal direction:

$$T = \sigma_1 A_1 + \sigma_2 A_2 \tag{4}$$

Combining both equations results in the following:

$$\begin{aligned} \sigma_{a1} &= \frac{T}{A_1 + A_2 \left(\frac{E_2}{E_1}\right)} \\ \sigma_{a2} &= \frac{T}{A_1 \left(\frac{E_2}{E_1}\right) + A_2} \end{aligned} \tag{5}$$

where  $\sigma_{a1}$  and  $\sigma_{a2}$  are the axial stresses of cable components 1 and 2, and  $A_1$  and  $A_2$  are the areas of cable components 1 and 2. The formulas for the tension and stress factors become:

$$\begin{aligned} K_{t1} &= \frac{1}{A_1 + A_2 \left(\frac{E_2}{E_1}\right)} \\ K_{t2} &= \frac{1}{A_1 \left(\frac{E_2}{E_1}\right) + A_2} \end{aligned} \tag{6}$$

An assumption is made to derive the equation for the curvature stress factor for copper and armor wires. A total of 100% utilization of the cable capacity with zero tension is assumed to be equal to reaching the limit of any of the materials in the cable due to curvature. From the capacity curve, the maximum curvature of the cable can be determined. The following formulas are established for estimating a conservative curvature stress factor for two different cable components:

$$\begin{aligned} K_{c1} &= Y_1 / C_{max} \\ K_{c2} &= Y_2 / C_{max} \end{aligned} \tag{7}$$

where  $Y_1$  and  $Y_2$  are the yield strengths of components 1 and 2, and  $C_{max}$  is the maximum allowable curvature of the cable.

The results obtained from the stress factor method are compared with those from the validated software, UFLEX. The stress factors are calculated through a detailed analysis of the stresses of the different cable components. Several axial tension and curvature loads are applied to analyze the stress distribution among the cable components.

### 2.4.3. Dynamic and Fatigue Damage Analysis

Dynamic analyses are performed for all load cases in each loading direction in OrcaFlex. All load-case simulations have a duration of one hour and a time step of 0.1 s. Each simulation uses a different random seed to enable independent wave and wind conditions. All load cases are considered for the fatigue analysis with their occurrence probabilities. Furthermore, all cases of one loading direction are scaled to the appearance probability of each loading direction. The simulations determine the axial tensions and the curvatures for each node along the power cable. Marine growth is considered by running two different fatigue analyses with the power cable in the SOL and EOL states.

The fatigue analysis is performed using the rainflow counting method [43]. This method uses the stress time history resulting from the dynamic analyses to calculate the fatigue damage. The stress reversal points are grouped into different stress ranges. In the rainflow counting method, four reversal points are considered to detect stress cycles. If the outer points bind the inner points, a cycle is counted, and the difference between the stress ranges of the inner points is assigned as the amplitude of this cycle. This method assumes that the fatigue damage resulting from a closed cycle in the irregular amplitude loading equals the fatigue damage caused by one cycle in a constant amplitude test. The damage caused by half-cycles is neglected in this procedure because there are few of them in every realistic case.

The cumulative damage is calculated according to the Miner–Palmgren rule [44]. This theory assumes constant damage during a given stress range. The following formula expresses the Miner–Palmgren rule:

$$D = \sum_{i=1}^k \frac{n_i}{N_i} \tag{8}$$

where  $D$  is the accumulated damage,  $i$  is a specific stress range, and  $k$  is the total number of stress ranges. Additionally,  $n$  is the number of cycles counted in a specific stress range, and  $N$  is the number of cycles until damage occurs in a specific stress range. The values for the different power cable components for  $N$  are obtained from the S–N curves. Based on these formulas, the fatigue damage and the fatigue life in years of the dynamic power cable can be determined.

### 3. Results and Discussion

This section shows the results of the estimated nonlinear bending behavior, the calculated fatigue damage, and the fatigue life. Moreover, the results from the proposed method for calculating the stress factors are compared with those obtained from the finite element simulations.

#### 3.1. Nonlinear Bending Behavior

Figure 7 shows the bending behavior for the selected power cable for curvatures from 0 to 0.1 m<sup>-1</sup> and different axial tension levels. The bending moment increases faster per unit curvature for small curvatures from 0 up to 0.015 m<sup>-1</sup> than for curvatures larger than this value for all applied tensions. The bending moment continues to increase linearly for curvatures higher than the ones stated in the figure until at least 0.2 m<sup>-1</sup>. Based on the results from Hu et al. [11], it increases similarly until the minimum bending radius of the cable is reached. The bending moment increases with higher axial tensions. As the baseline in this study, the curve for 50 kN axial tension is selected for the cable behavior since the cable usually has tensions around this value. Figure 8 shows the bending moment on different axes of the power cable. The bending moments are slightly higher for curvatures around the z-axis than for curvatures around the y-axis. These results align with the nonlinear bending behavior described by Hu et al. [11]. In their study, the layout of the cable cross-section with the three helically wound copper wire layers is stated as the reason for this nonlinearity.

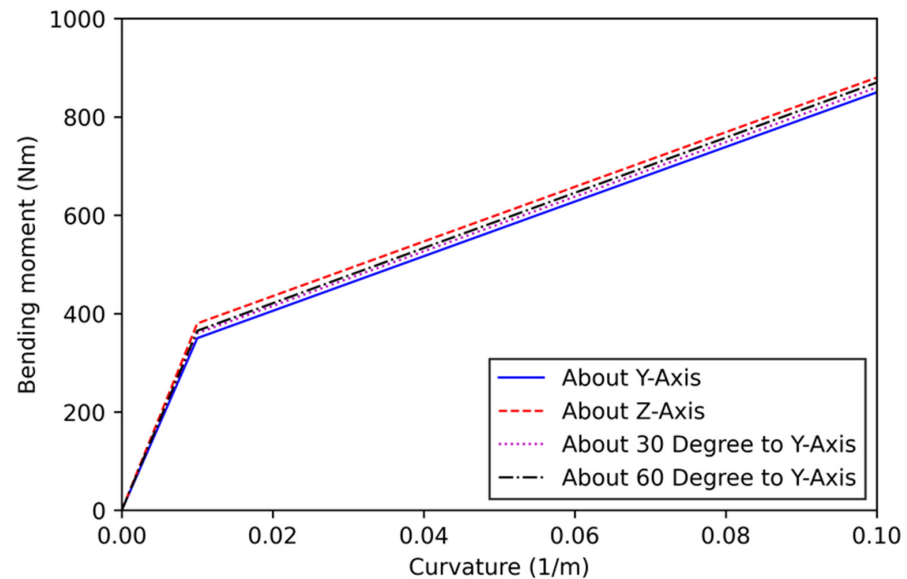


Figure 8. Nonlinear bending behavior of the power cable for different rotations.

### 3.2. Results Obtained by the Stress Factor Calculation Methods

Based on the formulas proposed by the present study, the stress factors described in Table 7 are obtained. The stress factors obtained with the finite element simulations are listed in Table 8. Figure 9 shows the results from the finite element simulations for 50 kN axial loading and  $0.1\text{ m}^{-1}$  curvature loading. The stresses are higher for armored steel wires than copper wires. This is because steel has a higher Young's modulus and higher yield strength than copper. Figures 10 and 11 compare the stresses resulting from the calculations with the stress factors and the finite element simulations for different axial loadings. The stresses obtained from the different calculation methods are similar for the copper and steel armor wires. Figures 12 and 13 show the stresses obtained by the two methods for different curvatures. A low axial load of 5 kN is applied in the finite element simulations to achieve faster convergence. The proposed stress factor method also assumes the same axial tension to enable a better comparison. The results show that the stresses obtained from the proposed stress factor calculation method are up to 218% higher for the copper and armor steel wires than those obtained from the finite element simulations. Considering that the calculation for the curvature stress factors is based on the maximum allowable curvature of the cable the manufacturer provides, which most likely contains a significant safety factor, higher values than obtained by finite element simulations can be expected. Additional curves assuming utilization factors as given in API 17J [45] are included in the figures. It can be concluded that the curvature stress factors are very conservative when calculated by the method proposed in the present study.

**Table 7.** Stress factors were obtained from the proposed method.

Components	Tension Stress Factor, Kt	Curvature Stress Factor, Kc
	(kPa/kN)	(kPa/(1/m))
Copper wires	232.3	360,000
Armor steel wires	489.0	1,080,000

**Table 8.** Stress factors were obtained from the finite element simulations.

Components	Tension Stress Factor, Kt	Curvature Stress Factor, Kc
	(kPa/kN)	(kPa/(1/m))
Copper wires	232.3	150,000
Armor steel wires	489.0	500,000

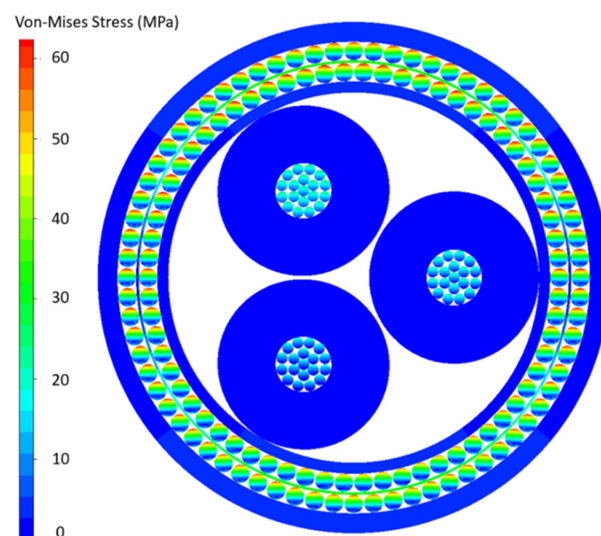


**Figure 9.** Finite element results for axial tension and curvature loads for 50 kN axial and  $0.1\text{ m}^{-1}$  curvature loading.

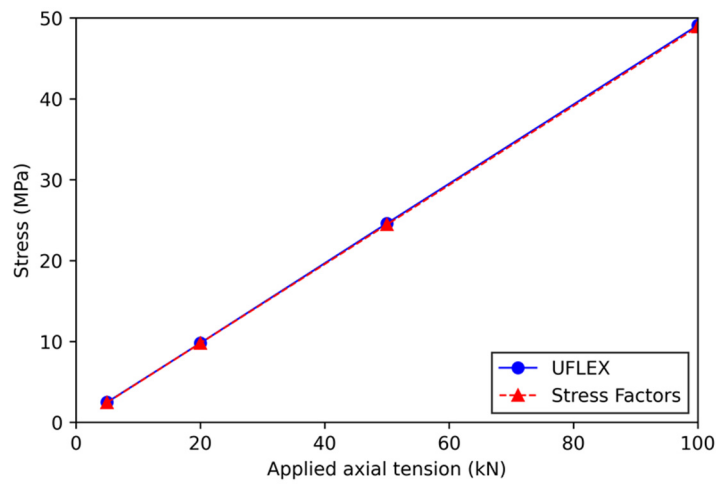


Figure 10. Armor wire stresses are obtained from different axial loads.

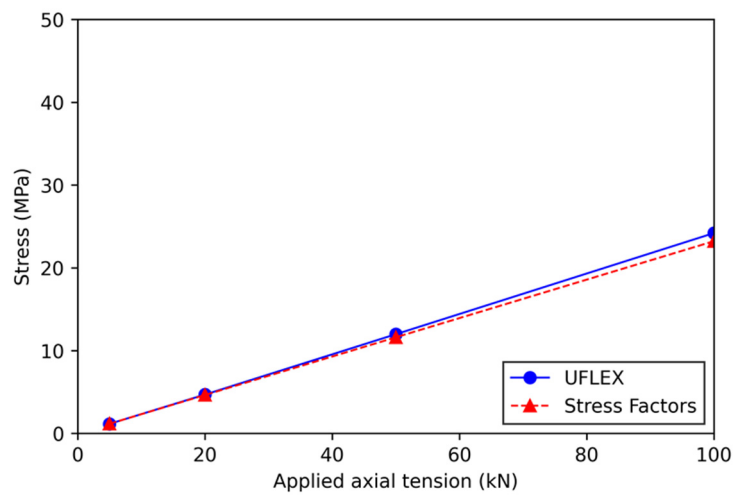


Figure 11. Copper wire stresses are obtained from different axial loads.

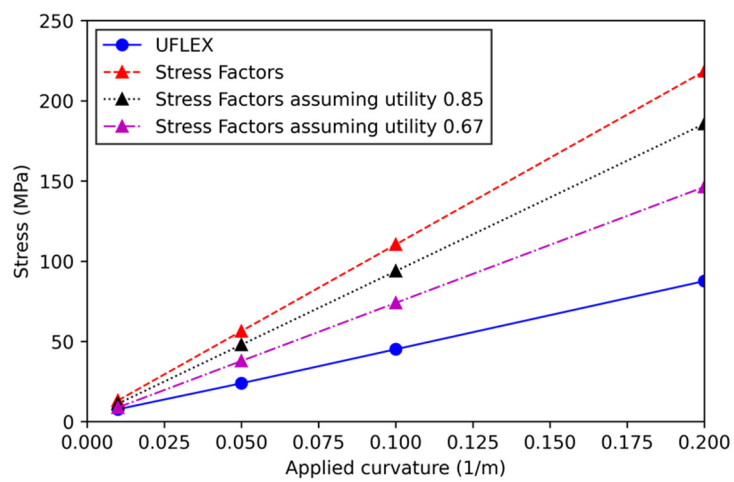


Figure 12. Armor wire stresses are obtained from different curvatures with 5 kN axial tension.

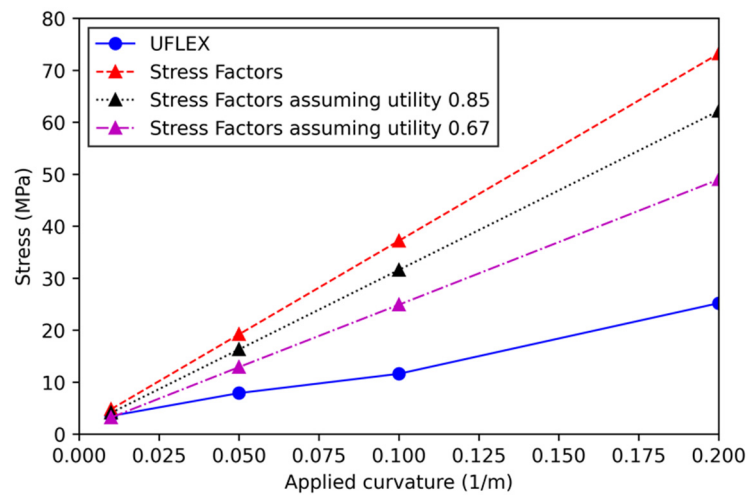


Figure 13. Copper wire stresses are obtained from different curvatures with 5 kN axial tension.

A sensitivity study on the friction effects of the cable components in the finite element software is carried out. Table 9 shows the results from the finite element simulations for a model including friction effects between the internal components and for a model neglecting these effects. The results of the two models are similar, with the setup including friction always resulting in slightly higher stress values. The differences between the two models are larger for the copper wires than for the armor steel wires. Additionally, the percentual deviation of the stresses obtained with the model neglecting friction effects compared to the ones obtained with the other model seems to decrease for higher curvatures.

Table 9. Friction affects the stresses of the cable components.

Specified Loads	Model Including Friction (MPa)		Zero-Friction Model (MPa)		Deviation (Zero-Friction to Friction)	
	Armor	Copper	Armor	Copper	Armor	Copper
20 kN axial, 0.05 1/m curvature	31.9	12.4	31.1	10.7	−2.5%	−13.7%
50 kN axial, 0.1 1/m curvature	68.2	26.7	67.1	23.9	−1.6%	−10.5%
50 kN axial, 0.2 1/m curvature	110.0	37.9	109.7	36.2	−0.3%	−4.5%

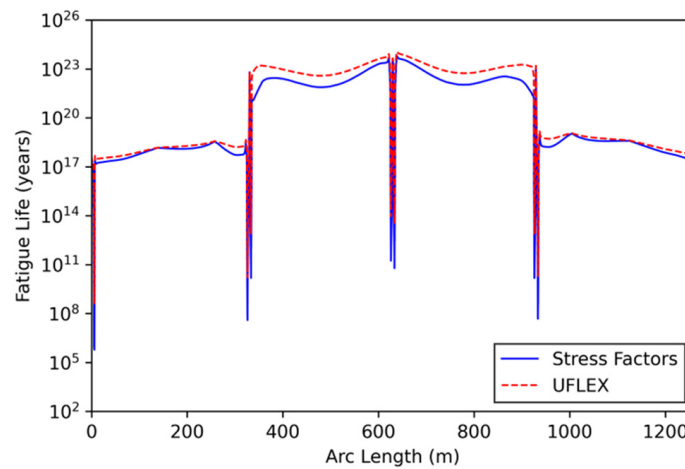
### 3.3. Fatigue Analysis Results

Table 10 shows the fatigue analysis results performed in OrcaFlex using the stress factors obtained by the method proposed in the present study and from the finite element software. The lowest fatigue life is identified for both marine growth states at the same location, close to the hang-off point. Very long fatigue lifetimes are obtained, indicating small tension and curvature ranges in the power cable. The failing components are the copper wires due to their lower resistance against long-cycle fatigue. The calculated lifetime for the EOL state is a maximum of 10% lower than for the SOL state. Figures 14 and 15 show the fatigue life over the cable length for the armor steel wires and the copper conductor in the SOL state, while Figures 16 and 17 show the EOL state results. The fatigue damage is significantly lower for the armor wires along the entire cable length than for the copper wires. The critical locations are identical for all analyzed cases, with the largest fatigue damage occurring close to the hang-off points and the buoys. Figure 18 shows the locations with the largest fatigue damage along the suspended power cable. Close to the ends of the power cable, the lifetime for the EOL state is lower than for the SOL state since the cable is in a depth zone with marine growth effects. However, no difference between the two states occurs in the middle parts of the power cable because the deeper location prevents marine

growth. Moreover, the figures show the results of the fatigue analyses performed with the stress factors obtained from the proposed simplified method and UFLEX. As expected, the fatigue life obtained using the new method's factors is lower for all components and marine growth states, confirming that it is a conservative approach. The lowest fatigue life occurs at the location with the largest curvature range. Therefore, bending is the main contributor to fatigue damage to the power cable in this configuration.

**Table 10.** Fatigue results based on the proposed stress factor calculation method.

Marine Growth State	Minimum Fatigue Life (Years)	Component	Location (m)	Location (Angle)
SOL	$71.06 \cdot 10^3$	Copper Wires	5.85	90°
EOL	$65.90 \cdot 10^3$	Copper Wires	5.85	90°



**Figure 14.** Fatigue life of the armor wires in the SOL state.

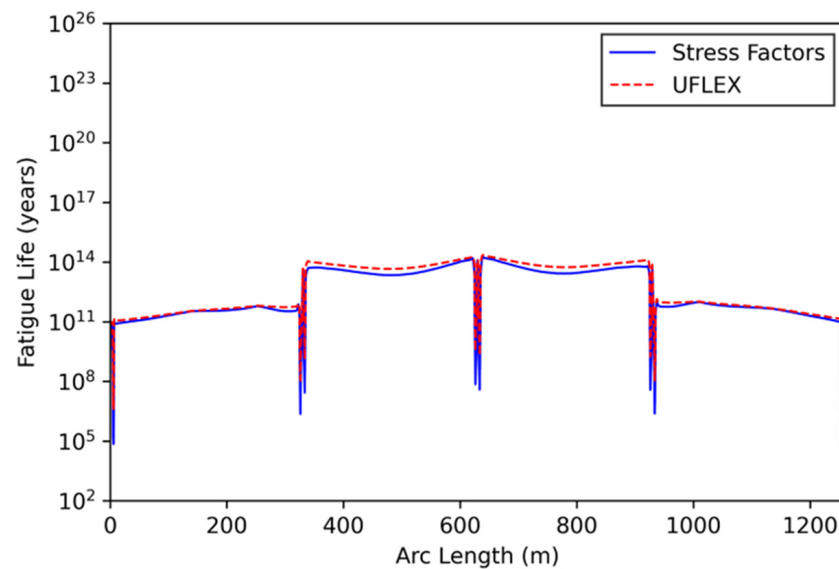


**Figure 15.** Fatigue life of the copper wires in the SOL state.



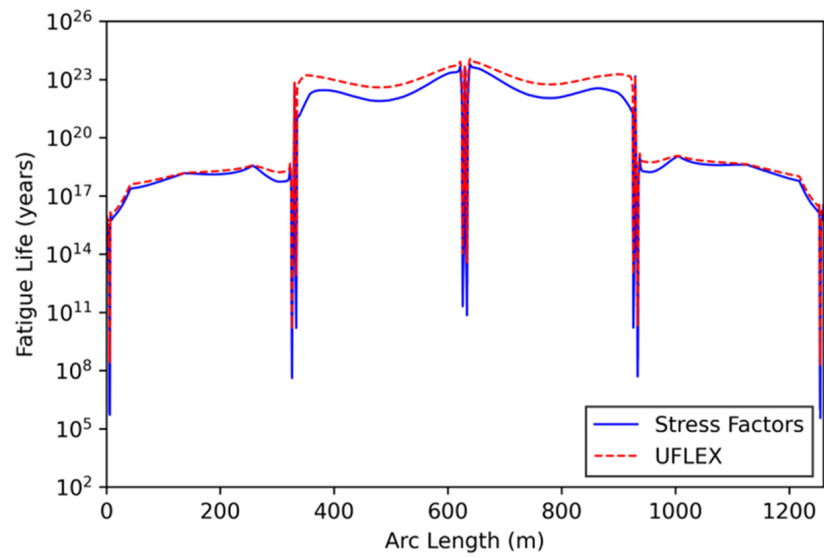


Figure 16. Fatigue life of the armor wires in the EOL state.

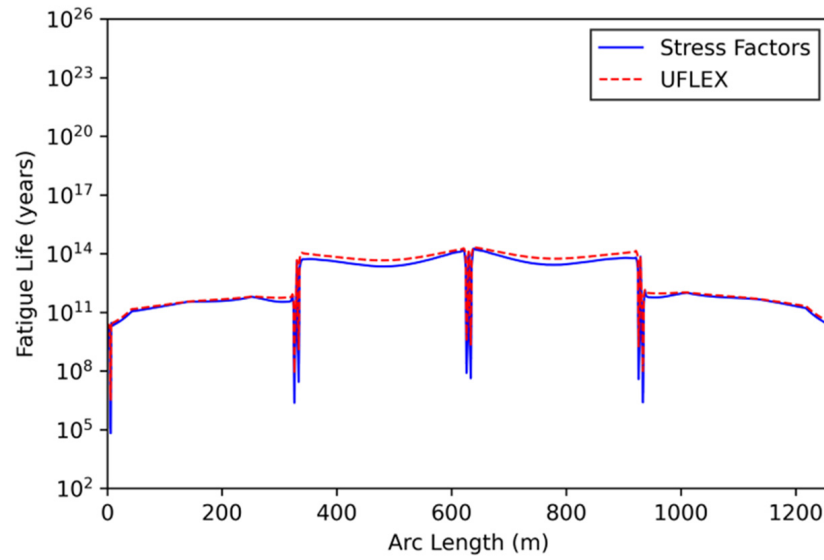


Figure 17. Fatigue life of the copper wires in the EOL state.

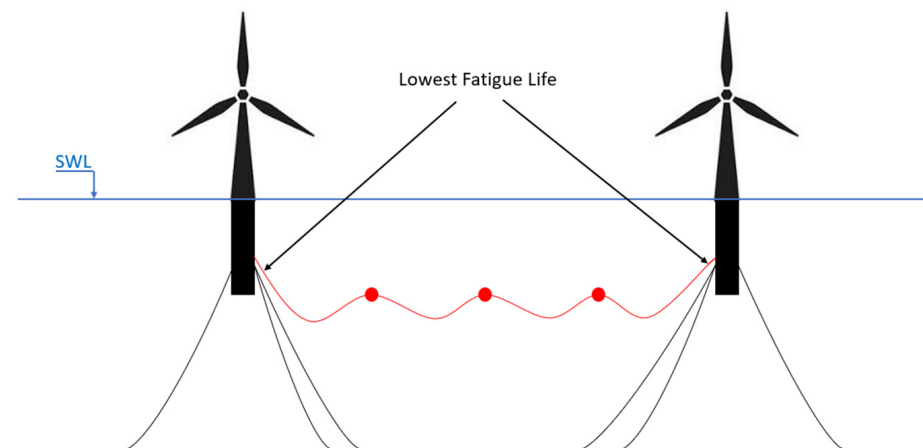


Figure 18. Locations of the lowest fatigue life along the suspended power cable.

#### 4. Conclusions

The fatigue life of a suspended inter-array power cable connecting two FOWTs is investigated considering environmental conditions in the North Sea. The fatigue calculation is based on stress factors estimated through a simplified method proposed in the present work for preliminary design. This method is based on composite beam stress theory and the minimum bending radius of the power cable. The applicability of this method is shown by validation with results from finite element simulations.

The main findings from the comparison of the stress factor calculation methods are:

- The proposed stress factor calculation method delivers good results for the selected cable when only tension is applied, based on the comparison with the results from the established finite-element software.
- The proposed stress factor calculation method delivers conservative results when curvature is applied in addition to tension.
- The proposed stress factor estimation method gives conservative results for the preliminary design of the power cable before more reasonable stress factors are known. The fatigue life should be calculated again after the stress factors are obtained through finite element software or experiments.

The main findings from the fatigue analysis of the suspended power cable configuration are:

- The suspended inter-array power cable in the presented configuration has a very long fatigue life resulting from low cyclic loadings.
- The critical areas with respect to fatigue damage are located next to the hang-off points and the buoys. Bending is identified as the main contributor to fatigue damage.
- The estimated fatigue life of the power cable is dependent on the cable and buoy properties. Therefore, the fatigue life should be calculated for each power cable configuration individually.
- The effects of marine growth on the power cable fatigue life are small because large parts of the power cable are located in depths where no marine growth occurs.

**Author Contributions:** Conceptualization, D.B., A.S. and M.C.O.; methodology, D.B., A.S., S.V.S. and M.C.O.; software, D.B. and A.S.; validation, D.B., A.S., S.V.S. and N.Y.; formal analysis, D.B.; investigation, D.B. and A.S.; resources, M.C.O. and N.Y.; data curation, D.B. and A.S.; writing—original draft preparation, D.B.; writing—review and editing, D.B., A.S., S.V.S., N.Y. and M.C.O.; visualization, D.B.; supervision, A.S., M.C.O. and N.Y. All authors have read and agreed to the published version of the manuscript.

**Funding:** This research is partially funded by the Research Council of Norway (project number 320902).

**Institutional Review Board Statement:** Not applicable.

**Informed Consent Statement:** Not applicable.

**Data Availability Statement:** Not applicable.

**Acknowledgments:** The authors would like to thank Nexans Norway AS for providing the properties of the power cable utilized in the present study. The authors would like to thank Morten Grøva from SINTEF Ocean for his help in using the finite-element software UFLEX.

**Conflicts of Interest:** The authors declare no conflict of interest.

#### References

1. Lee, J.; Zhao, F. GWEC-Global-Wind-Report. 2022. Available online: <https://gwec.net/wp-content/uploads/2022/03/GWEC-GLOBAL-WIND-REPORT-2022.pdf> (accessed on 6 June 2023).
2. Cozzi, L.; Wanner, B.; Donovan, C.; Toril, A.; Yu, W. Offshore Wind Outlook 2019: World Energy Outlook Special Report. 2019. Available online: [https://iea.blob.core.windows.net/assets/495ab264-4ddf-4b68-b9c0-514295ff40a7/Offshore\\_Wind\\_Outlook\\_2019.pdf](https://iea.blob.core.windows.net/assets/495ab264-4ddf-4b68-b9c0-514295ff40a7/Offshore_Wind_Outlook_2019.pdf) (accessed on 6 June 2023).
3. Eldøy, S. Hywind Scotland Pilot Park Project Plan for Construction Activities. 2017. Available online: <https://marine.gov.scot/sites/default/files/00516548.pdf> (accessed on 6 June 2023).

4. Principle Power Inc. WindFloat Atlantic. Available online: <https://www.principlepower.com/projects/windfloat-atlantic> (accessed on 17 November 2022).
5. Equinor ASA PUD Hywind Tampen. 2019. Available online: <https://www.equinor.com/content/dam/statoil/documents/impact-assessment/hywind-tampen/equinor-hywind-tampen-pud-del-II-konsekvensutredning-mars-2019.pdf> (accessed on 6 June 2023).
6. Rentschler, M.U.T.; Adam, F.; Chainho, P. Design Optimization of Dynamic Inter-Array Cable Systems for Floating Offshore Wind Turbines. *Renew. Sustain. Energy Rev.* **2019**, *111*, 622–635. [CrossRef]
7. Ikhennicheu, U.; Lynch, M.; Doole, S.; Borisade, F.; Wendt, F.; Schwarzkopf, M.-A.; Matha, D.; Vicente, R.D.; Tim, H.; Ramirez, L.; et al. *D3.1 Review of the State of the Art of Dynamic Cable System Design*; Corewind: Brussels, Belgium, 2020.
8. Thies, P.R.; Johannning, L.; Smith, G.H. Assessing Mechanical Loading Regimes and Fatigue Life of Marine Power Cables in Marine Energy Applications. *Proc. Inst. Mech. Eng. Part O J. Risk Reliab.* **2012**, *226*, 18–32. [CrossRef]
9. Thies, P.R.; Harrold, M.; Johannning, L.; Grivas, K.; Georgallis, G. Load and Fatigue Evaluation for 66 KV Floating Offshore Wind Submarine Dynamic Power Cable. 2019. Available online: [https://ore.exeter.ac.uk/repository/bitstream/handle/10871/40728/Thies\\_et%20al\\_JICABLE2019.pdf?sequence=1&isAllowed=y](https://ore.exeter.ac.uk/repository/bitstream/handle/10871/40728/Thies_et%20al_JICABLE2019.pdf?sequence=1&isAllowed=y) (accessed on 6 June 2023).
10. Bakken, K. Fatigue of Dynamic Power Cables Applied in Offshore Wind Farms. Master's Thesis, NTNU, Trondheim, Norway, 2019.
11. Hu, H.; Yan, J.; Sævik, S.; Ye, N.; Lu, Q.; Bu, Y. Nonlinear Bending Behavior of a Multilayer Copper Conductor in a Dynamic Power Cable. *Ocean. Eng.* **2022**, *250*, 110831. [CrossRef]
12. Svensson, G. Fatigue Prediction Models of Dynamic Power Cables by Laboratory Testing and FE Analysis. Master's Thesis, NTNU, Trondheim, Norway, 2020.
13. Zhao, S.; Cheng, Y.; Chen, P.; Nie, Y.; Fan, K. A Comparison of Two Dynamic Power Cable Configurations for a Floating Offshore Wind Turbine in Shallow Water. *AIP Adv.* **2021**, *11*, 39221. [CrossRef]
14. Ballard, B.; Yu, Y.-H.; Rij, J.V.; Driscoll, F. Umbilical Fatigue Analysis for a Wave Energy Converter. In Proceedings of the ASME 2020 39th International Conference on Ocean, Offshore and Arctic Engineering, Online, 3–7 August 2020.
15. Karlsen, S.; Slora, R.; Heide, K.; Lund, S.; Eggertsen, F.; Osborg, P.A. Dynamic Deep Water Power Cables. RAO/CIS OFFSHORE. 2009. Available online: [https://books-fmf.clan.su/\\_ld/1/101\\_DYNAMICDEEPWATE.pdf](https://books-fmf.clan.su/_ld/1/101_DYNAMICDEEPWATE.pdf) (accessed on 6 June 2023).
16. Marta, M.; Mueller-Schuetze, S.; Ottersberg, H.; Feu, I.D.; Johannning, L.; Thies, P.R. Development of Dynamic Submarine MV Power Cable Design Solutions for Floating Offshore Renewable Energy Applications. 2015. Available online: [https://ore.exeter.ac.uk/repository/bitstream/handle/10871/18314/JICABLE15\\_0144\\_final.pdf?sequence=1&isAllowed=y](https://ore.exeter.ac.uk/repository/bitstream/handle/10871/18314/JICABLE15_0144_final.pdf?sequence=1&isAllowed=y) (accessed on 6 June 2023).
17. Nasution, F.P.; Sævik, S.; Gjøsteen, J.K.Ø. Fatigue Analysis of Copper Conductor for Offshore Wind Turbines by Experimental and FE Method. *Energy Procedia* **2012**, *24*, 271–280. [CrossRef]
18. Nasution, F.P.; Sævik, S.; Gjøsteen, J.K.Ø. Finite Element Analysis of the Fatigue Strength of Copper Power Conductors Exposed to Tension and Bending Loads. *Int. J. Fatigue* **2014**, *59*, 114–128. [CrossRef]
19. Yang, S.-H.; Ringsberg, J.W.; Johnson, E. Parametric Study of the Dynamic Motions and Mechanical Characteristics of Power Cables for Wave Energy Converters. *J. Mar. Sci. Technol.* **2018**, *23*, 10–29. [CrossRef]
20. Rapha, J.I.; Domínguez, J.L. Suspended Cable Model for Layout Optimisation Purposes in Floating Offshore Wind Farms. *J. Phys. Conf. Ser.* **2021**, *2018*, 012033. [CrossRef]
21. Schnepf, A.; Lopez-Pavon, C.; Ong, M.C.; Yin, G.; Johnsen, Ø. Feasibility Study on Suspended Inter-Array Power Cables between Two Spar-Type Offshore Wind Turbines. *Ocean. Eng.* **2023**, *277*, 114215. [CrossRef]
22. Schnepf, A.; Devulder, A.; Johnsen, Ø.; Ong, M.C.; Lopez-Pavon, C. Numerical Investigations on Suspended Power Cable Configurations for Floating Offshore Wind Turbines in Deep Water Powering an FPSO. *J. Offshore Mech. Arct. Eng.* **2023**, *145*, 030904. [CrossRef]
23. Ahmad, I.B.; Schnepf, A.; Ong, M.C. An Optimization Methodology for Suspended Inter-Array Power Cable Configurations between Two Floating Offshore Wind Turbines. *Ocean. Eng.* **2023**, *277*, 114406. [CrossRef]
24. Orcina Ltd. OrcaFlex. Available online: <https://www.orcina.com/webhelp/OrcaFlex/> (accessed on 4 April 2023).
25. Python Software Foundation. Python v3.10. Available online: <https://www.python.org/> (accessed on 17 November 2022).
26. SINTEF. *Uflex2D Version 2.8 Theory Manual*; SINTEF Ocean: Trondheim, Norway, 2018.
27. Sævik, S.; Bruaseth, S. Theoretical and Experimental Studies of the Axisymmetric Behaviour of Complex Umbilical Cross-Sections. *Appl. Ocean. Res.* **2005**, *27*, 97–106. [CrossRef]
28. Dai, T.; Sævik, S.; Ye, N. Comparison Study of Umbilicals' Curvature Based on Full Scale Tests and Numerical Models. In Proceedings of the 26th International Ocean and Polar Engineering Conference, Rhodes, Greece, 26 June 2016; p. 6.
29. Sævik, S.; Gjøsteen, J.K.Ø. Strength Analysis Modelling of Flexible Umbilical Members for Marine Structures. *J. Appl. Math.* **2012**, *2012*, 985349. [CrossRef]
30. SINTEF. Uflex Software—Fact Sheet. 2017. Available online: [https://www.sintef.no/globalassets/sintef-ocean/pdf/uflexfactsheet\\_2017\\_des.pdf](https://www.sintef.no/globalassets/sintef-ocean/pdf/uflexfactsheet_2017_des.pdf) (accessed on 6 June 2023).
31. Jonkman, J.; Butterfield, S.; Musial, W.; Scott, G. Definition of a 5-MW Reference Wind Turbine for Offshore System Development. National Renewable Energy Laboratory; 2009. Available online: <https://www.nrel.gov/docs/fy09osti/38060.pdf> (accessed on 6 June 2023).
32. Jonkman, J. Definition of the Floating System for Phase IV of OC3. National Renewable Energy Laboratory; 2010. Available online: <https://www.nrel.gov/docs/fy10osti/47535.pdf> (accessed on 6 June 2023).

33. Nexans Norway AS Subsea Composite Cable OM1052 2022.
34. DNV. *GL AS DNVGL-RP-0005 RP-C203: Fatigue Design of Offshore Steel Structures*; DNV: Høvik, Norway, 2014.
35. Standards Norway. *NORSOK N-003—Actions and Action Effects*; NORSOK Standards: Oslo, Norway, 2007.
36. DNV. *DNV-RP-C205: Environmental Conditions and Environmental Loads*; DNV: Høvik, Norway, 2010.
37. Spyrou, C.; Mitsakou, C.; Kallos, G.; Louka, P.; Vlastou, G. An Improved Limited Area Model for Describing the Dust Cycle in the Atmosphere. *J. Geophys. Res.* **2010**, *115*, D17211. [[CrossRef](#)]
38. Komen, G.J.; Cavaleri, L.; Donelan, M.; Hasselmann, K.; Hasselmann, S.; Janssen, P.A.E.M. *Dynamics and Modelling of Ocean Waves*; Cambridge University Press: Cambridge, MA, USA, 1994.
39. WAMDI Group. The WAM Model—A Third Generation Ocean Wave Prediction Model. *J. Phys. Oceanogr.* **1988**, *12*, 1775–1810.
40. Papadopoulos, A.; Nickovic, S.; Missirlis, N. The ETA Model Operational Forecasting System and Its Parallel Implementation. *Notes Numer. Fluid Mech.* **1997**, *62*, 176–188.
41. Asplin, L.; Albretsen, J.; Johnsen, I.A.; Sandvik, A.D. The Hydrodynamic Foundation for Salmon Lice Dispersion Modeling along the Norwegian Coast. *Ocean. Dyn.* **2020**, *70*, 1151–1167. [[CrossRef](#)]
42. Gramoll, K. *Mechanics—Theory*. Available online: [https://www.ecourses.ou.edu/cgi-bin/ebook.cgi?topic=me&chap\\_sec=06.1&page=theory](https://www.ecourses.ou.edu/cgi-bin/ebook.cgi?topic=me&chap_sec=06.1&page=theory) (accessed on 18 November 2022).
43. ASTM. *International Practices for Cycle Counting in Fatigue Analysis*; American Petroleum Institute: Washington, DC, USA, 2011.
44. Kauzlarich, J.J. The Palmgren-Miner Rule Derived. In *Tribology Series*; Elsevier: Amsterdam, The Netherlands, 1989; Volume 14, pp. 175–179. ISBN 978-0-444-87435-1.
45. API. *API 17J: Specification for Unbonded Flexible Pipe*; American Petroleum Institute: Washington, DC, USA, 2008.

**Disclaimer/Publisher’s Note:** The statements, opinions and data contained in all publications are solely those of the individual author(s) and contributor(s) and not of MDPI and/or the editor(s). MDPI and/or the editor(s) disclaim responsibility for any injury to people or property resulting from any ideas, methods, instructions or products referred to in the content.